Synthetic Metals 161 (2011) 2460–2465

Contents lists available at SciVerse ScienceDirect

Synthetic Metals

journal homepage: www.elsevier.com/locate/synmet

Porous graphene/carbon nanotube composite cathode for proton exchange membrane fuel cell

Young Soo Yun [a], Doyoung Kim [b], Yongsug Tak [b], Hyoung-Joon Jin [a,*]

[a] Department of Polymer Science and Engineering, Inha University, Incheon 402-751, Republic of Korea
[b] Department of Chemical Engineering, Inha University, Incheon 402-751, Republic of Korea

ARTICLE INFO

Article history:
Received 11 July 2011
Received in revised form
15 September 2011
Accepted 15 September 2011
Available online 11 October 2011

Keywords:
Cathodes
Carbon nanotubes
Graphenes
Proton exchange Membrane fuel cell

ABSTRACT

Porous Pt-graphene/multiwalled carbon nanotube (MWCNT) composite cathodes were fabricated for proton exchange membrane fuel cells and their electro-chemical performances were examined. Rod-like MWCNTs with a high aspect ratio induced a porous network structure and Pt-graphene was bound homogeneously to the porous network structure of MWCNTs in the form of a very rough surface, which facilitated simultaneous access between the Pt electro-catalyst and reactant. In addition, the porous MWCNT network enabled the Pt-graphene electrode to overcome the deficiency induced by high electrical resistance by providing an electrical pathway for the oxygen reduction reaction (ORR). Therefore, the ORR charge transfer resistance of the Pt-graphene/MWCNT composite cathode was much smaller than that of the Pt-graphene cathode, and the maximum power density of the Pt-graphene/MWCNT composite cathode was four times higher than that of the Pt-graphene cathode.

1. Introduction

Proton exchange membrane fuel cells (PEMFCs) utilizing hydrogen as a fuel are being developed to replace batteries in portable electronic devices and internal combustion engines in automobiles on account of their high energy efficiency, low pollutant emission and low working temperature. In PEMFCs, Pt-based electro-catalysts are widely used as anode and cathode electro-catalysts for hydrogen oxidation and oxygen reduction reaction (ORR), respectively. One important goal for the commercialization of PEMFCs is to reduce the amount of Pt electro-catalysts required without sacrificing the performance. To effectively utilize the Pt electro-catalysts, the Pt must have simultaneous access to the gas, electron-conducting medium, and proton-conducting medium. Therefore, the catalyst layers must be relatively thin to minimize the losses due to the rate of proton diffusion within the catalyst layer and the rate of mass transfer of the chemical reactants and products to and from the active sites. The latter can contribute to a significant overpotential or polarization of the electrodes, which can limit the cell performance, particularly at high current densities [1]. A range of methods, such as modified thin film methods [2], sputter deposition [3], electrodeposition [4], electrospray techniques [5] and Pt sol methods [6], have been used to achieve high Pt utilization and better performance. However, many challenges still remain [7].

Various carbon materials with different nanostructures and morphological characteristics have been used as the electro-catalyst supports in PEMFCs [8–12]. The catalytic activity of the Pt based electro-catalysts is strongly dependent on the catalyst support, which plays a very important role in determining the size and degree of catalyst dispersion as well as the distribution and stabilization of catalyst particles [12]. Instead of traditional carbon supports for the electro-catalysts, nano-sized carbon supports can be used effectively to reduce the Pt loading.

Graphene, which is a one-atom-thick two-dimensional layer of sp^2-bonded carbon, has attracted considerable attention owing to its unique physical, chemical and electrical properties [13–15]. The unique nanostructure and properties have potential applications in electro-chemical devices [16–18]. Graphene sheets used for electro-catalytic ORR showed higher performance and electro-chemical surface areas (ESAs) than the commercial catalyst, E-TEK [19]. However, electrodes prepared by graphene have an obstacle in mass transfer of the chemical reactants and products to and from the active sites due to graphene's morphological characteristics [20]. Therefore, a new strategy for mass transfer of graphene electrodes is required when a thin catalyst layer using graphene sheets is fabricated.

Carbon nanotubes (CNTs) are some of the most promising materials for the design of functional thin films, including those for catalytic membranes [21,22] and for a range of electro-chemical energy conversion and storage devices [23–25] owing to

* Corresponding author. Tel.: +82 32 860 7483; fax: +82 32 865 5178.
E-mail address: hjjin@inha.ac.kr (H.-J. Jin).

0379-6779/$ – see front matter © 2011 Elsevier B.V. All rights reserved.
doi:10.1016/j.synthmet.2011.09.030

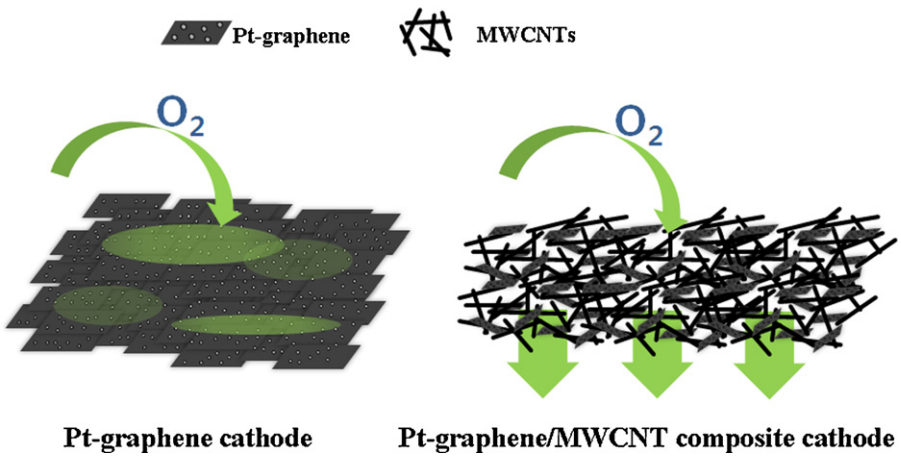

Fig. 1. The structures of the Pt-graphene cathode and Pt-graphene/MWCNT composite cathode.

their unique morphological characteristics and physical properties, including one-dimensional high aspect ratio, large surface area, high electrical conductivity, and superior chemical and mechanical stability [26,27]. Nano-structured membranes fabricated by CNTs, which allow fast mass transfer, were prepared using several methods, such as layer by layer assembly [28], templated growth [29,30], vacuum filtering [31,32] and spinning technology [33].

In this study, porous Pt-graphene/multiwalled carbon nanotubes (MWCNTs) composite cathodes were prepared for PEMFCs and their electro-chemical performance was examined. A porous network structure of a Pt-graphene/MWCNT composite cathode was formed by spray coating from a Pt-graphene and MWCNT dispersion. The porous network structure induced by the MWCNTs acted as a pathway for mass transfer of the chemical reactants and products and as an electrical bridge. Therefore, Pt-graphene/MWCNT composite cathodes showed higher performance for PEMFC than did Pt-graphene cathodes. Fig. 1 shows a schematic diagram of the structures of the Pt-graphene cathode and the Pt-graphene/MWCNT composite cathode.

2. Experimental

2.1. Fabrication of acid treated MWCNTs and graphene oxides (GOs)

The as-received MWCNTs (NCT, Japan) were treated with acid using a procedure reported elsewhere [32]. Briefly, the MWCNTs were treated in an acid mixture (sulfuric acid/nitric acid = 3:1 (v/v) at 60 °C for 18 h.

The GOs were prepared from natural graphite (Sigma–Aldrich) using the Hummers method. Aqueous GO suspensions were frozen in liquid nitrogen and then freeze-dried using a lyophilizer (LP3, Jouan, France) at −50 °C and 0.045 mbar for 72 h. After lyophilization, low density, loosely packed GO powders were obtained.

2.2. Fabrication of the Pt-graphene

The graphene supported Pt catalysts were prepared by the modified microwave-assisted polyol process described by Fang et al. [12]. In particular, 5.0 mL of an aqueous solution of 0.05 M $H_2PtCl_6{\cdot}6H_2O$ was mixed with 150 mL of ethylene glycol in a 250 mL beaker. A total of 1.75 mL of 0.4 M KOH was then added dropwise to a vigorously stirred solution to adjust the pH to approximately 8–9. The required amount of GOs was added to the mixture and ultrasonicated for 30 min. The beaker containing the mixture of Pt salts and GOs was heated in a household microwave oven (SAMSUNG RE-C20DV, 2450 MHz, 700 W) for 100 s. The resulting suspension was stirred vigorously overnight and filtered. The residue (mainly graphene-supported Pt catalyst) was washed thoroughly with deionized water and dried overnight at 80 °C.

2.3. Preparation of the Pt-graphene cathode and the Pt-graphene/MWCNT composite cathode

The fabricated Pt-graphene was dispersed in isopropyl alcohol by an ultrasound treatment for 30 min and then mixed with a 5 wt% Nafion solution. The mixture was then ultrasonicated for another 30 min and sprayed onto a carbon cloth. In the case of the Pt-graphene/MWCNT composite cathode, both the fabricated Pt-graphene and MWCNTs were dispersed in isopropyl alcohol by ultrasound treatment for 30 min and then mixed with a 5 wt% Nafion solution. The mixture was then ultrasonicated for a further 30 min and then sprayed onto a carbon cloth. A 50 wt% Pt loaded carbon black catalysts (J&M) was also prepared using a similar method.

2.4. Preparation of membrane electrode assembly (MEA)

The 50 wt% Pt loaded carbon black catalysts (J&M) were used as the anode catalysts. The electrodes had a geometric area of 4 cm^2 with a Pt loading of 0.2 mg/cm^2. The Pt-graphene cathode and Pt-graphene/MWCNT composite cathode had geometric areas of 4 cm^2 with a Pt loading of 0.13 mg/cm^2. The MEA was prepared by hot-pressing a pretreated Nafion 212 (DuPont) sandwiched by the anode and cathode.

2.5. Characterization

The morphologies of the MWCNTs and electrodes were observed by field emission scanning electron microscopy (FESEM, S-4300SE, Hitachi, Japan) at an accelerating voltage of 15 kV after precoating the samples with a homogeneous Pt layer by ion sputtering (E-1030, Hitachi, Japan). The morphologies of GO and Pt-graphene were observed by transmission electron microscopy (TEM, CM200, Philips, USA) and atomic force microscopy (AFM, a Digital Instrument Nanoscope IVA). X-ray diffraction (XRD, Rigaku DMAX 2500) of the Pt-graphene was carried out using Cu Kα radiation (wavelength λ = 0.154 nm) operated at 40 kV and 100 mA. X-ray photoelectron spectroscopy (XPS, PHI 5700 ESCA) was performed using monochromated Al Kα radiation ($h\nu$ = 1486.6 eV). To estimate the ESA of Pt in the carbon-supported Pt catalysts, a three-electrode electrochemical cell was employed, and cyclic voltammetry (CV)

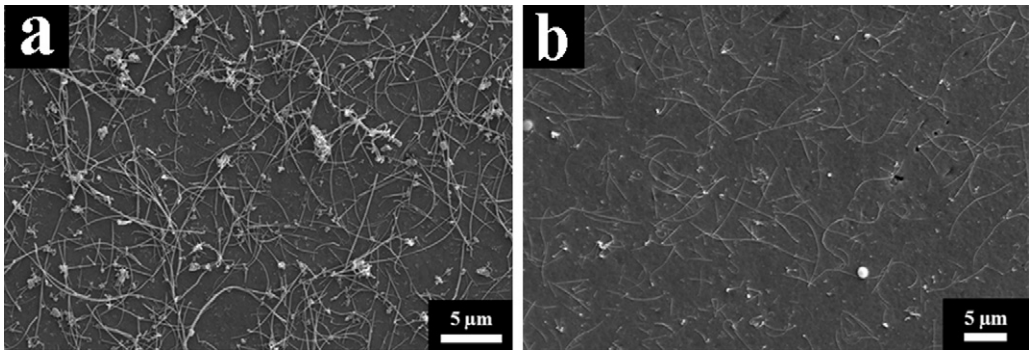

Fig. 2. SEM images of (a) pristine MWCNTs and (b) acid treated MWCNTs.

measurements were taken at room temperature with a scan rate of 50 mV/s over the potential range, 0.1–1.4 V (vs. NHE), under a 50 cm^3/min H_2 flow in the anode and 50 cm^3/min O_2 flow in the cathode. Polarization performance tests were conducted at 70 °C with a constant current and with a fuel cell test station. H_2 and O_2 were supplied to the anode and cathode at a flow rate of 200 and 600 mL/min, respectively.

3. Results and discussion

MWCNTs would have a straight shape because the MWCNTs consist of rolled graphene layers. However, heptagon–pentagon pair and other pairs, which are generated during the MWCNT synthesis process, bend the tube permanently. Therefore, MWCNTs have a range of morphologies with respect to their degree of bending [34,35]. Rod-like MWCNTs with a high aspect ratio were used to prepare porous Pt-graphene composite membranes [34,35]. The MWCNTs were treated with strong acid to disperse in hydrophilic media and to purify the carbonaceous impurities and metallic catalysts. The acid treatment also induces morphological changes as a result of a cutting process [32,36]. Fig. 2 shows the morphologies of the pristine and acid treated MWCNTs. The pristine MWCNTs were entangled with each other and contained carbonaceous impurities and metallic catalysts. Although pristine MWCNTs have a high aspect ratio, they exhibit a relatively short end-to-end distance compared to their contour lengths and high bending ratio. In contrast, the acid treated MWCNTs have a relatively long end-to-end distance and low bending ratio due to the cutting process by acid attack [36]; most carbonaceous impurities and metallic catalysts were also removed by the acid treatment. As a result, the MWCNTs obtained by the acid treatment had a high aspect ratio, low sheet resistance, contour length and bending ratio of 127, 7.6×10^{-1} Ω/□, 4747 nm and 0.85, respectively [32,34,35]. Fig. 3 shows the morphology of the GO prepared from graphite using the Hummers method. GO has wrinkles and folds on the edges with a thickness of 1.6 nm, which corresponds to a few layers of graphene with functional groups [37]. Pt nano-particles were incorporated onto the graphene surfaces (Fig. 4). All the graphene sheets were coated uniformly with the nano-sized Pt nano-particles with little aggregation, even at a high metal loading of 50 wt%, indicating a strong interaction between the graphene support and particles. These Pt nanoparticles attached to the graphene surface can prevent the graphene from aggregating and restacking. The mean Pt nano-particle sizes on graphene sheets estimated from the TEM images were 2–3 nm. Fig. 5(a) shows XRD patterns of Pt-graphene. The mean Pt nano-particle size, which was estimated from the isolated Pt (2 2 0) peak using the Scherrer equation (Eq. (1)), was 2.2 nm, which was consistent with the typical TEM images of the Pt-graphene samples.

$$L = \frac{0.9\ \lambda_{K\alpha 1}}{B_{(2\theta)} \cos\theta_{max}} \quad (1)$$

where $\lambda_{K\alpha 1}$ is the X-ray wavelength; θ_{max} is the maximum angle of the (2 2 0) peak; $B_{(2\theta)}$ is the half-peak width for Pt (2 2 0) in radians.

Fig. 5(b) shows the high-resolution C 1s XPS spectra of GO and Pt-graphene. The C 1s XPS spectrum of GO clearly shows a considerable degree of oxidation. The peak of oxygenated functional groups was decreased after reducing GO by ethylene glycol with chloroplatinic acid [38]. Graphene reduced by ethylene glycol recovered its electro-conductivity, from 10^8 Ω/□ to 10^4 Ω/□.

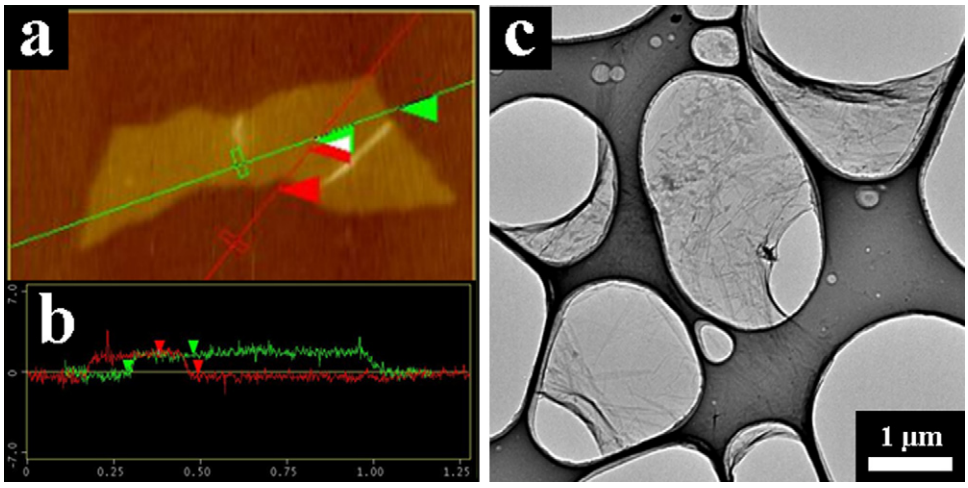

Fig. 3. (a and b) AFM data and (c) TEM image of graphene oxide.

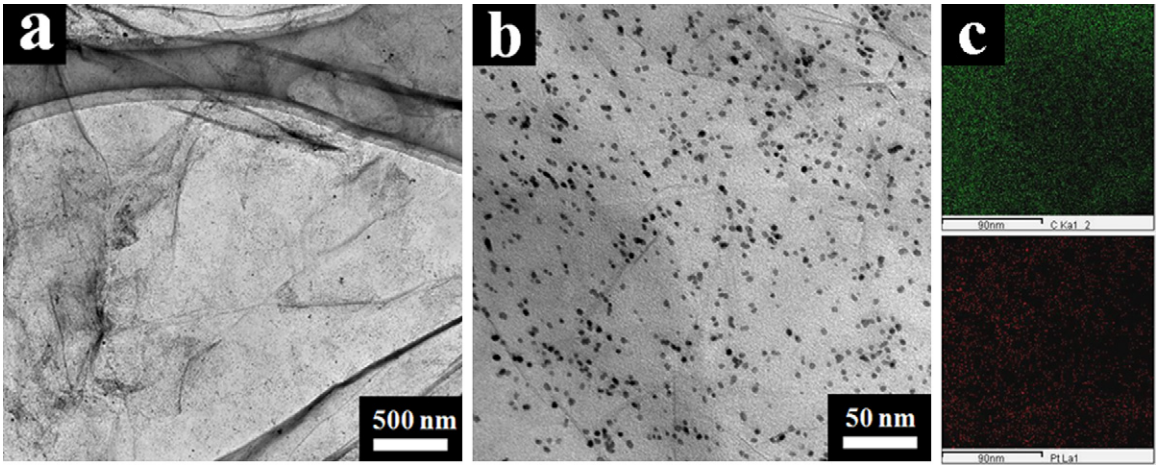

Fig. 4. (a and b) TEM images and (c) EDX data of Pt-graphene (Pt loading: 50 wt%).

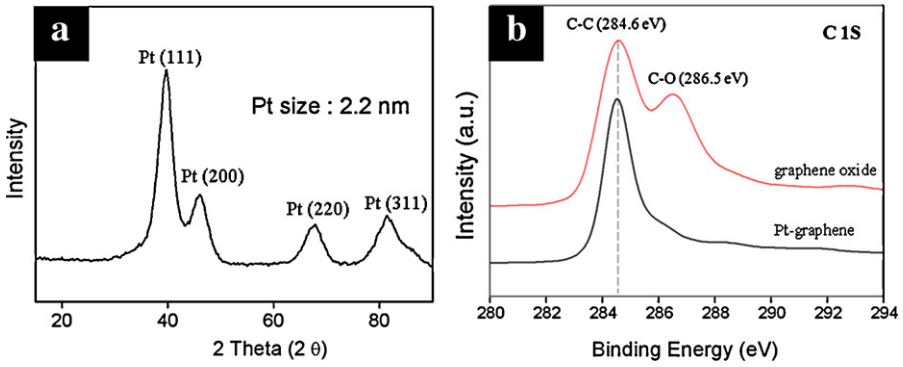

Fig. 5. (a) XRD pattern of Pt-graphene and (b) typical C 1s XPS spectra of graphene oxide and Pt-graphene.

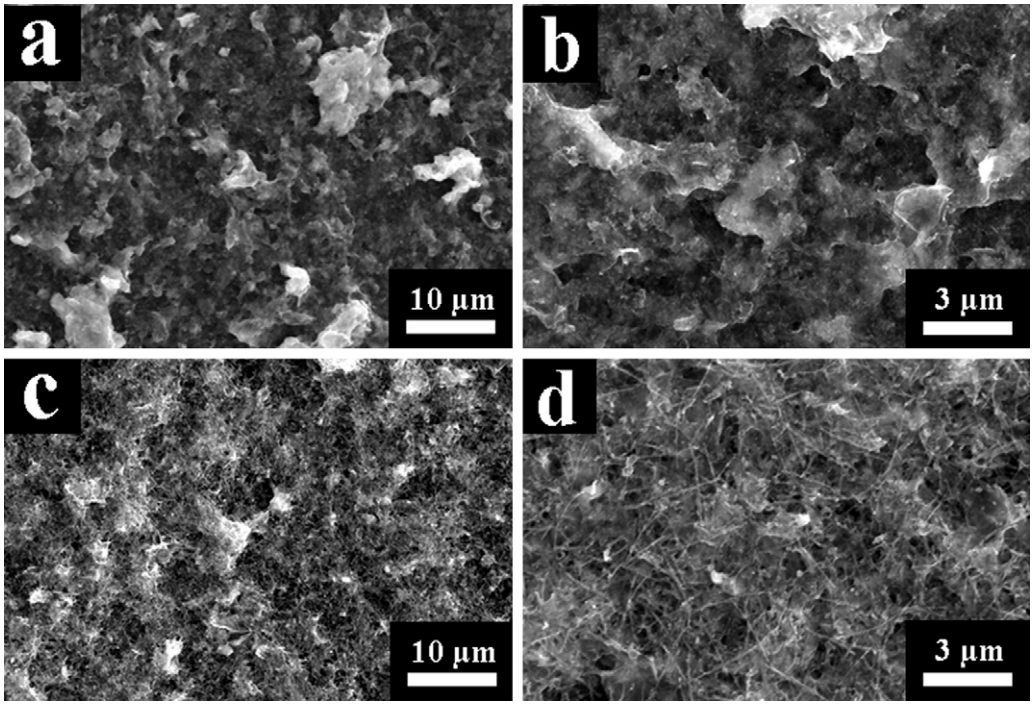

Fig. 6. SEM images of the surface morphology of (a and b) Pt-graphene electrode and (c and d) Pt-graphene/MWCNT composite electrode.

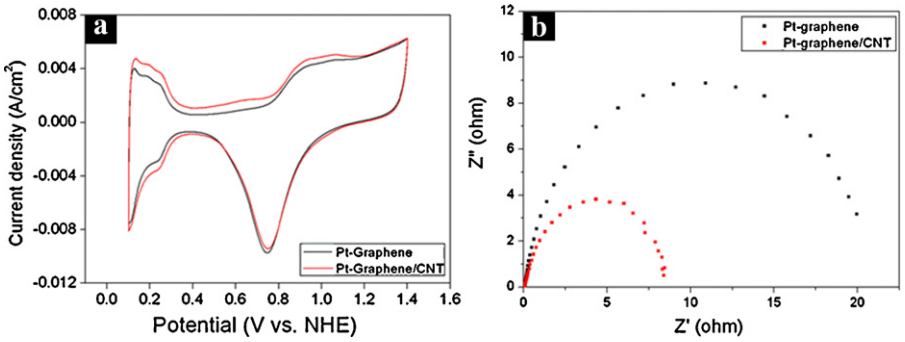

Fig. 7. (a) Cyclic voltammograms of 50 wt% Pt-graphene cathode and Pt-graphene/MWCNT composite cathode at a scan rate of 50 mV/s over a potential range of 0.1–1.4 V (0.13 mg Pt/cm^2) and (b) Nyquist plots for the 50 wt% Pt-graphene cathode and the 50 wt% Pt-graphene/MWCNT composite cathode (0.13 mg Pt/cm^2), frequency range from 2000 Hz to 0.05 Hz with an amplitude of 1 mA at 70 °C in OCV condition.

However, this level is not enough to apply to electrodes. Fig. 6 shows the morphologies of Pt-graphene electrode (Fig. 6a and b) and Pt-graphene/MWCNT composite electrode (Fig. 6c and d). In the case of the Pt-graphene electrode, Pt-graphene is densely packed and appears to be non-porous. In contrast, the MWCNT-incorporated Pt-graphene electrode has a porous structure because of the interconnected MWCNTs. Pt-graphene is bound homogeneously to the network structure of MWCNTs and has a rougher surface, which facilitates simultaneous access among the Pt electro-catalyst, reactant and Nafion. The extension of three-phase boundary results in an enhancement of the ORR electrocatalytic activity. In addition, the MWCNT network provides an electrical pathway for ORR. This enables the Pt-graphene electrode to overcome the deficiency induced by the high electrical resistance. Fig. 7(a) shows the cyclic voltammograms of the Pt-graphene and Pt-graphene/MWCNT composite cathode at a scan rate of 50 mV/s over the potential range of 0.1–1.4 V. ESAs of the Pt in the supported Pt (50 wt%) catalysts were determined from the integrated charge (after subtracting the capacitance contribution) in the hydrogen absorption region of the steady-state cyclic voltammograms in a supporting electrolyte.

$$\text{ESA}\ \ [\text{cm}^2/\text{g of Pt}] = \frac{\text{Charge}\ \ [Q_H, \mu\text{C/cm}^2]}{210\ \ [\mu\text{C/cm}^2] \times \text{electrode loading}\ \ [\text{g of Pt/cm}^2]} \quad (2)$$

According to Eq. (2), the ESA was calculated to be 38.2 m^2/g for Pt in the Pt-graphene/MWCNT composite cathode, which was slightly larger than the 34.5 m^2/g for Pt in the Pt-graphene cathode, indicating the higher utilization efficiency of the Pt-graphene/MWCNT composite cathode due to the effects induced by the MWCNTs. However, there were no significant differences between the two electrodes. Since the two electrodes were manufactured to have the same Pt mass and used the same catalyst supports, the electrochemical surface areas of the Pt electro-catalysts could be similar despite the presence of MWCNTs in the cathode. The ORR electrocatalytic activities of the Pt-graphene and Pt-graphene/MWCNT composite cathode were evaluated by Nyquist plots, as shown in Fig. 7(b). The Nyquist plots in Fig. 6(b) conform to the ORR electrocatalytic activity in the cathode because the components of the single cell are the same except for the cathode. The semicircular diameter of the Pt-graphene/MWCNT composite cathode plot was much smaller than that of the Pt-graphene cathode plot. This suggests that the ORR charge transfer resistance was much smaller at the Pt-graphene/MWCNT composite cathode catalysts. Fig. 8 shows the polarization curves of the Pt-carbon black cathode, Pt-graphene/MWCNT composite cathode and Pt-graphene cathode. In the very low current density region, a rapid voltage drop in the potential–current curve, which is generally known as activation polarization, reflects the sluggish kinetics intrinsic to the ORR at the cathode surface. The polarization voltage drop of the Pt-graphene/MWCNT composite cathode was slightly smaller than

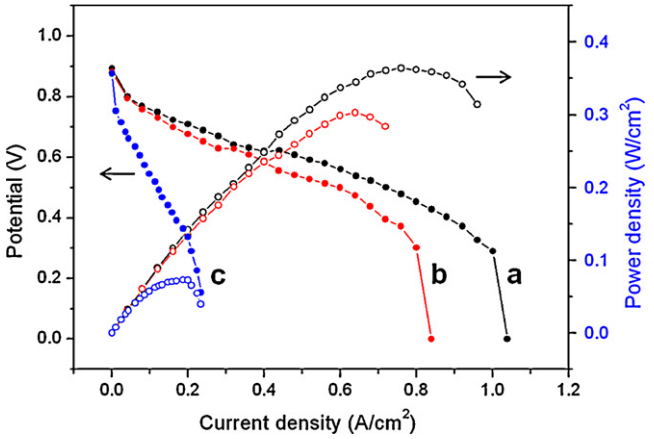

Fig. 8. (a) Polarization and power density plots at 70 °C of the PEMFCs using the 50 wt% Pt-carbon black cathode (0.2 mg Pt/cm^2), (b) the 50 wt% Pt-graphene/MWCNT composite cathode (0.13 mg Pt/cm^2) and (c) the 50 wt% Pt-graphene cathode (0.13 mg Pt/cm^2).

that of the Pt-graphene cathode. However, the Pt-graphene cathode exhibited a rapid voltage drop induced by both an ohmic drop and the mass transfer limitation at a relatively low current density region. The porous network structure in the Pt-graphene/MWCNT composite cathode provides a fast pathway to the active sites through which the reactant and products can be transported readily from the active sites, and by which they can avoid the mass transport limitation. In addition, the ohmic drop of the cathode induced by the high electrical resistance was decreased by the electrical bridge of the MWCNT network. Therefore, the performance of the Pt-graphene/MWCNT composite cathode is much higher than that of the Pt-graphene cathode. The maximum power densities for the Pt-graphene/MWCNT composite cathode and Pt-graphene cathode were 303 mW/cm^2 and 73 mW/cm, respectively. The maximum power density of the Pt-graphene/MWCNT composite cathode (0.13 mg Pt/cm^2) was only 17% lower than that of the Pt-carbon black cathode with a 35% higher Pt loading (0.2 mg Pt/cm^2). In addition, the maximum power density of the Pt-graphene/MWCNT composite cathode was increased four fold compared to that of the Pt-graphene cathode.

4. Conclusion

Porous Pt-graphene/MWCNT composite cathodes were prepared for PEMFCs and their electro-chemical performances were examined. Rod-like MWCNTs with a high aspect ratio of 127, low sheet resistance of $7.6 \times 10^{-1}\ \Omega/\square$, contour length of 4747 nm and bending ratio of 0.85 were used to make a porous network

structure. 2–3 nm sized Pt nano-particles with little aggregation, even at a high metal loading of 50 wt%, were incorporated homogeneously onto the graphene surfaces. Pt-graphene was bound homogeneously to the network structure of the MWCNTs; it has a very rough surface, which facilitates simultaneous access between Pt electro-catalyst and reactant. The ESA of the Pt in the Pt-graphene/MWCNT composite cathode was calculated to be 38.2 m^2/g, which is slightly larger than the 34.5 m^2/g for Pt in the Pt-graphene cathode. These results indicate better utilization efficiency of the Pt-graphene/MWCNT composite cathode due to effects induced by MWCNTs. However, there were no significant differences between the two electrodes. In the case of the ORR electrocatalytic activities evaluated by Nyquist plots, the ORR charge transfer resistance of the Pt-graphene/MWCNT composite cathode was much smaller than that of the Pt-graphene cathode. In addition, the maximum power density of the Pt-graphene/MWCNT composite cathode was found to increase four fold compared to that of the Pt-graphene cathode.

Acknowledgements

This work was supported by the National Research Foundation of Korea Grant funded by the Korean Government (MEST) (NRF-2010-C1AAA001-0029018), and a grant from the Korea Institute of Energy and Resources Technology Evaluation and Planning (KETEP) funded by the Korean government (2008-N-BL-HM-E-02-0000).

References

[1] A.L. Dicks, J. Power Sources 156 (2006) 128–141.
[2] L. Xiong, A. Manthiram, Electrochim. Acta 50 (2005) 3200–3204.
[3] D. Gruber, N. Ponath, J. Muller, F. Lindstaedt, J. Power Sources 150 (2005) 67–72.
[4] H. Kim, B.N. Popov, Electrochem. Solid State Lett. 7 (2004) A71–A74.
[5] R. Benıtez, J. Soler, L. Daza, J. Power Sources 151 (2005) 108–113.
[6] M.R. Khana, S.D. Lin, J. Power Sources 162 (2006) 186–191.
[7] J.-H. Wee, K.-Y. Lee, S.H. Kim, J. Power Sources 165 (2007) 667–677.
[8] E. Antolini, Appl. Catal. B: Environ. 88 (2009) 1–24.
[9] E.P. Ambrosio, C. Francia, M. Manzoli, N. Penazzi, P. Spinelli, Int. J. Hydrogen Energy 33 (2008) 3142–3145.
[10] C. Wang, M. Waje, X. Wang, J.M. Tang, R.C. Haddon, Y. Yan, Nano Lett. 4 (2004) 345–348.
[11] S. Litster, G. McLean, J. Power Sources 130 (2004) 61–76.
[12] B. Fang, J.H. Kim, M. Kim, J.-S. Yu, Chem. Mater. 21 (2009) 789–796.
[13] Y. Zhu, S. Murali, W. Cai, X. Li, J.W. Suk, J.R. Potts, R.S. Ruoff, Graphene and graphene oxide: synthesis, properties, and applications, Adv. Mater. 22 (2010) 3906–3924.
[14] S. Stankovich, D.A. Dikin, G.H.B. Dommett, K.M. Kohlhaas, E.J. Zimney, E.A. Stach, R.D. Piner, S.T. Nguyen, R.S. Ruoff, Nature 442 (2006) 282–286.
[15] Y.K. Koh, M.-H. Bae, D.G. Cahill, E. Pop, Nano Lett. 10 (2010) 4363–4368.
[16] B. Seger, P.V. Kamat, J. Phys. Chem. C 113 (2009) 7990–7995.
[17] A.L.M. Reddy, A. Srivastava, S.R. Gowda, H. Gullapalli, M. Dubey, P.M. Ajayan, ACS Nano 4 (2010) 6337–6342.
[18] S. Biswas, L.T. Drzal, Chem. Mater. 22 (2010) 5667–5671.
[19] R. Kou, Y. Shao, D. Wang, M.H. Engelhard, J.H. Kwak, J. Wang, V.V. Viswanathan, C. Wang, Y. Lin, Y. Wang, I.A. Aksay, J. Liu, Electrochem. Commun. 11 (2009) 954–957.
[20] O.C. Compton, S. Kim, C. Pierre, J.M. Torkelson, S.T. Nguyen, Adv. Mater. 22 (2010) 4759–4763.
[21] J.K. Holt, H.G. Park, Y. Wang, M. Stadermann, A.B. Artyukhin, C.P. Grigoropoulos, A. Noy, O. Bakajin, Science 312 (2006) 1034–1037.
[22] R. Smajda, A. Kukovecz, Z. Kony, I. Kiricsi, Carbon 45 (2007) 1176–1184.
[23] S.W. Lee, N. Yabuuchi, B.M. Gallant, S. Chen, B.-S. Kim, P.T. Hammond, Y. Shao-Horn, Nat. Nanotechnol. 5 (2010) 531–537.
[24] A. Izadi-Najafabadi, S. Yasuda, K. Kobashi, T. Yamada, D.N. Futaba, H. Hatori, M. Yumura, S. Iijima, K. Hata, Adv. Mater. 22 (2010) E235–E241.
[25] L. Hua, J.W. Choi, Y. Yang, S. Jeong, F.L. a Mantia, L.-F. Cui, Y. Cui, Proc. Natl. Acad. Sci. U.S.A. 106 (2009) 21490–21494.
[26] R.H. Baughman, A.A. Zakhidov, W.A.D. Heer, Science 297 (2002) 787–792.
[27] P.M. Ajayan, O.Z. Zhou, Carbon Nanotubes, Springer-Verlag, Berlin, 2001, pp. 391–425.
[28] S.W. Lee, B.-S. Kim, S. Chen, Y. Shao-Horn, P.T. Hammond, J. Am. Chem. Soc. 131 (2009) 671–679.
[29] J. Li, C. Papadopoulos, J.M. Xu, Appl. Phys. Lett. 75 (1999) 367–369.
[30] N. Halonen, A. Rautio, A.-R. Leino, T. Kyllonen, G. Toth, J. Lappalainen, K. Kordas, M. Huuhtanen, R.L. Keiski, A. Sapi, M. Szabo, A. Kukovecz, Z. Konya, I. Kiricsi, P.M. Ajayan, R. Vajtai, ACS Nano 4 (2010) 2003–2008.
[31] P.G. Whitten, G.M. Spinks, G.G. Wallace, Carbon 43 (2005) 1891–1896.
[32] Y.S. Yun, H. Bak, H.-J. Jin, Synth. Met. 160 (2010) 561–565.
[33] M. Zhang, K.R. Atkinson, R.H. Baughman, Science 206 (2004) 1358–1361.
[34] H.S. Lee, C.H. Yun, H.M. Kim, C.J. Lee, J. Phys. Chem. C 111 (2007) 18882–18887.
[35] Y.S. Yun, H.I. Kwon, H. Bak, E.J. Lee, J.-S. Yoon, H.-J. Jin, Macromol. Res. 18 (2010) 828–833.
[36] D.-Y. Kim, Y.S. Yun, H. Bak, S.Y. Cho, H.-J. Jin, Curr. Appl. Phys. 10 (2010) 1046–1052.
[37] G. Eda, G. Fanchini, M. Chhowalla, Nat. Nanotechnol. 3 (2008) 270–274.
[38] Y. Li, W. Gao, L. Ci, C. Wang, P.M. Ajayan, Carbon 48 (2010) 1124–1130.